phys. stat. sol. (b) **243**, No. 10, 2428–2435 (2006) / **DOI** 10.1002/pssb.200668080

Two-photon photoluminescence and exciton binding energies in single-walled carbon nanotubes

R. Pomraenke[*, 1], **J. Maultzsch**[2], **S. Reich**[3], **E. Chang**[4], **D. Prezzi**[4], **A. Ruini**[4], **E. Molinari**[4], **M. S. Strano**[5], **C. Thomsen**[2], and **C. Lienau**[1]

[1] Max-Born-Institut für Nichtlineare Optik und Kurzzeitspektroskopie, Max-Born-Str. 2a, 12489 Berlin, Germany
[2] Institut für Festkörperphysik, Technische Universität Berlin, Hardenbergstr. 36, 10623 Berlin, Germany
[3] Department of Materials Science and Engineering, Massachusetts Institute of Technology, 77 Massachusetts Avenue, Cambridge, MA 02139-4307, USA
[4] INFM National Research Center S3, and Physics Department, University of Modena and Reggio Emilia, via Campi 213/A, 41100 Modena, Italy
[5] University of Illinois, Department of Chemistry and Biomolecular Engineering, 600 South Mathews Avenue, Urbana, IL 61801, USA

Received 6 March 2006, revised 24 April 2006, accepted 24 April 2006
Published online 18 July 2006

PACS 71.35.–y, 73.22.–f, 78.47.+p, 78.55.Hx, 78.67.Ch, 78.67.Lt

We compare experimental one- and two-photon luminescence excitation spectra of single-walled carbon nanotubes at room temperature to *ab initio* calculations. The experimental spectra reveal a Rydberg-like series of excitonic states. The energy splitting between these states is a clear fingerprint of excitonic correlations in carbon nanotubes. From those spectra, we derive exciton binding energies of 0.3–0.4 eV for nanotubes with diameters between 6.8 Å and 9.0 Å. These energies are in quantitative agreement with our theoretical calculations, which predict the symmetries of the relevant excitonic wave functions and indicate that a low-lying optically dark excitonic state may be responsible for the low luminescence quantum yields in nanotubes.

1 Introduction

The influence of excitonic effects on linear and nonlinear optical spectra has been an important topic in carbon nanotube research during the last two years. Initially, when luminescence was discovered from individual nanotubes in stable aqueous solutions [1, 2], the optical absorption and luminescence spectra of carbon nanotubes were interpreted in terms of single-particle excitations [2], governed by the van-Hove singularities in the density of states of a quasi-one-dimensional system [3]. More recently, different theoretical studies have predicted that the Coulomb interaction between the excited electron and hole is strong and affects both the transition frequencies and the shape of the optical spectra [4–9], in analogy to previous experimental and theoretical studies on other, e.g., GaAs-based, quasi-one-dimensional systems [10]. In contrast to conventional bulk semiconductors, the strong quantum confinement of electron and hole in the quasi-one-dimensional nanotube was expected to result in large exciton binding energies. Values ranging from a few tens of meV to about 1 eV have been suggested, depending on tube diameter, chirality, and dielectric screening [5–7]. These theoretical predictions have recently triggered first ex-

* Corresponding author: e-mail: pomraenk@mbi-berlin.de, Phone: +49 30 6392 1471, Fax: +49 30 6392 1489

perimental studies using nonlinear optical spectroscopy to probe excitonic correlations [11–13] and binding energies of several hundred meV have been demonstrated.

Here, we give a detailed account of our experimental studies of one- and two-photon luminescence excitation spectra of single-walled carbon nanotubes and compare these results to first principles calculations of linear and nonlinear optical spectra. Together, experiment and theory show that optical spectra of these nanostructures are fully governed by excitonic correlations, and allow to extract exciton binding energies and symmetries of the optically active excitonic states.

2 Experimental

The concept of our experiment is outlined in Fig. 1(a). The idea is to make use of the different selection rules for one- and two-photon photoluminescence to specifically address excitonic states with different symmetry. In carbon nanotubes, one expects for each allowed interband transition a series of transitions to optically active exciton states with odd (u) symmetry with respect to rotations by π about the U axis of the tube [Fig. 1(a)]. Two-photon excitation couples to the otherwise optically inactive even (g) states [Fig. 1(b)]. The energetic splitting between the one- and two-photon active states indicates the strength of Coulomb correlations [14].

Experimentally, we use 100 fs laser pulses from a Ti:sapphire oscillator, operating at a repetition rate of 80 MHz and tunable between 700 and 970 nm for one-photon-excitation. The Ti:sapphire laser also pumps an optical parametric oscillator, delivering sub 150 fs pulses at 80 MHz repetition range in the wavelength range between 1150 and 2000 nm. For two-photon spectroscopy, these pulses are focussed to a spot size of about 3 μm into a solution of single-walled carbon nanotubes suspended in D_2O with sodium dodecyl sulfate as surfactant. The tubes were produced by the HiPCO method. Photoluminescence

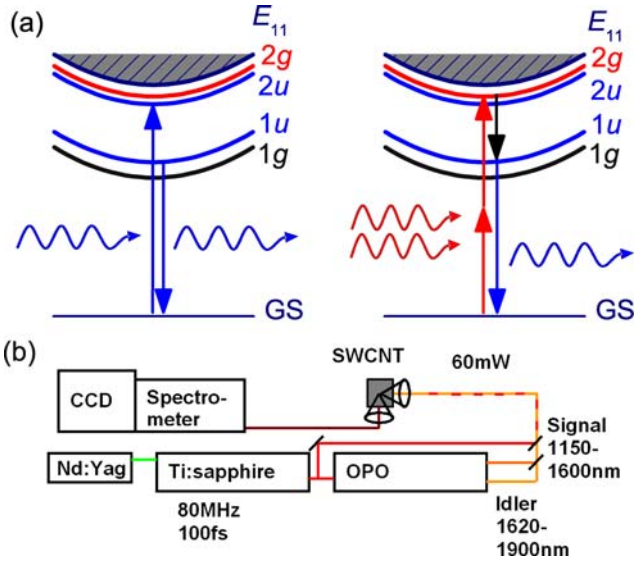

Fig. 1 (online colour at: www.pss-b.com) (a) Schematic picture of one-photon absorption and emission in carbon nanotubes. E_{11} indicates the single-particle transition between the lowest subbands. One-photon excitations couple to excitonic states with odd (u) symmetry with respect to π rotations about the U axis. The U axis is perpendicular to the tube axis through the center of the C hexagons [15]. (b) Schematic of the experimental setup. Spectrally tunable 100 fs laser pulses from a Ti:sapphire oscillator pumping an optical parametric oscillator are used for one- and two-photon excitation and focused into the nanotube solution using a microscope objective. Nanotube photoluminescence is collected at an angle of 90° with a second microscope objective, spectrally dispersed in a monochromator and detected with a CCD camera.

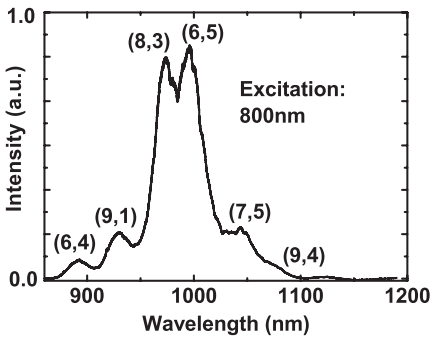

Fig. 2 Typical nanotube photoluminescence spectrum for one-photon excitation at 800 nm. Between 850 nm and 1070 nm the luminescence from 6 different nanotube species [(6,4), (9,1), (8,3), (6,5), (7,5) and (9,4)] is identified.

from the sample was collected in a 90° configuration using a second microscope objective, spectrally dispersed in an 0.5 m monochromator and detected with a liquid nitrogen cooled charge coupled (CCD) device. All experiments were performed at room temperature.

A typical photoluminescence spectrum of our nanotube sample for one-photon excitation at 800 nm is shown in Fig. 2. Between 850 and 1150 nm we can identify the luminescence from 6 different nanotube species [(6,4), (9,1), (8,3), (6,5), (7,5) and (9,4)]. The assignment of the chiral indices (n_1, n_2) of these tubes is based on previous Raman [16, 17] and luminescence [2] data. The steep decay of the luminescence intensity for wavelengths above 1050 nm is mainly given by the spectral sensitivity of the red-enhanced silicon-based CCD camera.

3 Results and discussion

Figure 3 shows a spectrally-resolved two-photon luminescence excitation spectrum of our sample for below band gap excitation between 1210 and 1970 nm. In these experiments, the excitation wavelength is changed in 10 nm steps by tuning the optical parametric oscillator. For each excitation wavelength the laser power is kept constant at 60 mW, corresponding to an excitation intensity of about 30 GW/cm^2 and the photoluminescence spectrum is integrated over 60 seconds. For each tube, we find a maximum in the luminescence intensity at an excitation wavelength far above the emission wavelength, but significantly smaller than twice this wavelength. We assign these absorption maxima to resonant two-photon excitation of the lowest two-photon allowed exciton state ($2g$). The positions of the maxima thus correspond to half the energy of this state. Emission results from relaxation into the lowest one-photon active $1u$ state [Fig. 1(a)]. The energetic shift between both states is a clear signature of the excitonic nature of the optical absorption and emission processes at room temperature. The magnitude of this shift of about

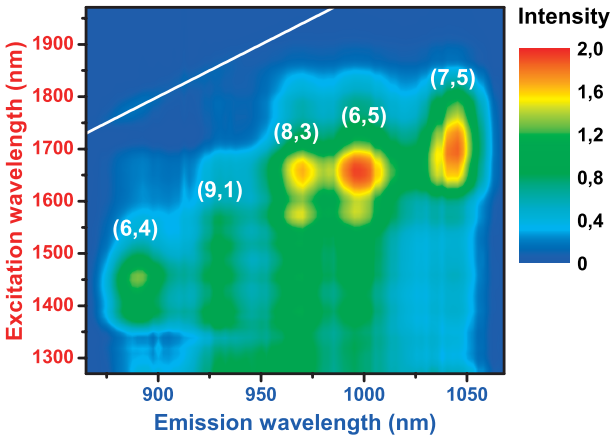

Fig. 3 (online colour at: www.pss-b.com) Two-photon luminescence excitation spectra of carbon nanotubes. The luminescence intensity is plotted as a function of excitation and detection wavelength. The sample is excited with spectrally tunable 150 fs laser pulses with 60 mW average power, focussed to a spot size of 3 μm.

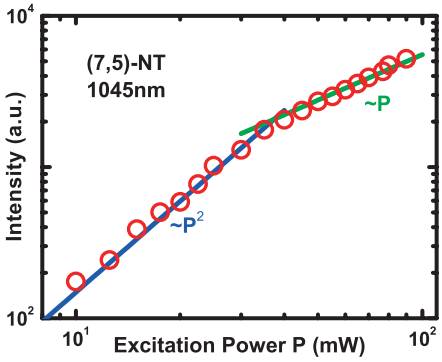

Fig. 4 (online colour at: www.pss-b.com) Excitation-power (in mW) dependence of the two-photon luminescence intensity. The power dependence is recorded for the (7,5) tube emitting at 1045 nm for an excitation wavelength of 1720 nm.

240–320 meV shows that exciton binding energies in carbon nanotubes correspond to almost one fourth of the band-gap energy. An analysis of the power dependence of the emission intensity supports the assignment to two-photon absorption (Fig. 4). At low excitation powers, the luminescence intensity increases indeed quadratically. We observe a saturation into a linear increase above 40 mW, showing that the spectra in Fig. 3 are in fact recorded in the linear intensity regime.

For a quantitative analysis, we directly compare one- and two-photon spectra for the same nanotube in Fig. 5. In these spectra, the emission intensity is plotted as a function of the excess energy, i.e, $E^{ex} - E_{11}^{1u} = \hbar\omega - E_{11}^{1u}$ for one-photon, and $2\hbar\omega - E_{11}^{1u}$ for two-photon excitation, respectively. The two-photon spectrum simply shows a single resonance, roughly 240 meV above the luminescent state. Similar spectra and splittings (between 240 and 325 meV) are also found for the other nanotubes species investigated. They are in agreement with recent experimental findings in Ref. [12]. Interestingly, the one-photon luminescence excitation spectrum of the (7,5) tube also shows a weak resonance at an excess energy of 200 meV, i.e., only slightly below the first two-photon resonance at 240 meV. The same resonance is also observed in the excitation spectrum of the second subband (E_{22}). This makes it very likely that all these resonances reflect one-photon excitation of higher-lying exciton states. Alternative suggestions for the origin of these peaks, e.g., phonon sidebands and exciton-phonon excitations [18, 19], appear less likely.

A quantitative interpretation of these experimental results requires an adequate theoretical description of the optical spectra. Such a description is challenging because of the large number of atoms in the carbon nanotube unit cell. We use the approach reported in Ref. [5] which fully accounts for the nanotube helical symmetry. We start from single-particle wave functions obtained by density functional theory and

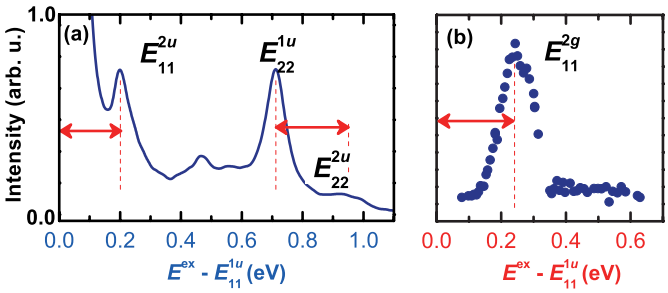

Fig. 5 (online colour at: www.pss-b.com) Comparison of one-photon (a) and two-photon (b) luminescence excitation spectra of the (7,5) tube emitting at 1045 ± 5 nm. The abscissa gives the difference between the absorption and emission energy. For one-photon absorption, E_{11} and E_{22} indicate the first- and second-subband transitions, respectively. The peak at 0.2 eV is assigned to the $2u$ exciton resonance. In two-photon absorption, the $2g$ state is excited at 0.24 eV above the $1u$ emission, pointing to an exciton binding energy of about 300 meV.

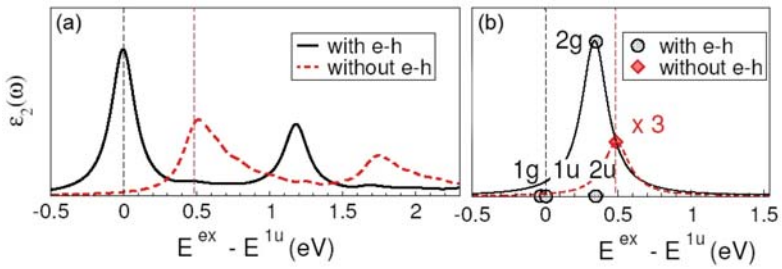

Fig. 6 (online colour at: www.pss-b.com) *Ab initio*-calculated (a) one-photon and (b) two-photon absorption for the (6,4) tube with a Lorentzian broadening of 0.1 eV. Black solid (red dashed) lines are with (without) electron–hole (e–h) interactions. The black circles in two-photon absorption denote the probability amplitude for two-photon scattering to the exciton states 1*g*, 1*u*, 2*u*, and 2*g*. The probability amplitude of scattering to the final state without e–h interaction is indicated by a red diamond.

adopt the GW approximation for the self-energy operator [20]. The optical properties are then calculated by solving the Bethe–Salpeter equation (BSE) for the two-particle electron–hole excitations. The BSE is expanded in a localized Gaussian basis set which is symmetric with respect to the screw axis of the tube. This approach allows us to calculate wave functions and binding energies of bound electron–hole pairs [21–23]. It gives a symmetry characterization of the excited states including their optical selection rules.

One- and two-photon absorption spectra for the (6,4) tube, calculated using this approach in the presence and absence of exciton interactions, are shown in Fig. 6 on the same energy axis as in Fig. 5. In the absence of electron-hole interaction, both one- and two-photon spectra show peaks at an energy corresponding to the difference between the lowest nanotube subband in the conduction and valence band, E_{11}. In the one-photon spectrum, the spectral shape reflects the one-dimensional density of states, apart from the finite broadening of the spectrum. In the calculations, a relatively large broadening of 100 meV was assumed to account for both homogeneous and inhomogeneous broadening in the experimental spectra. Switching on the electron–hole interaction shifts the lowest one-photon active transition strongly to the red, indicating an exciting binding energy of 0.50 eV. The shape of this spectrum reflects the excitonic density of the states and their broadening, the free carrier continuum is almost completely suppressed. As in the experiment, the two-photon spectrum essentially shows a single resonance, 340 meV above the lowest one-photon active resonance, and below the E_{11} energy.

The theoretical calculations not only provide a quantitative description of our experimental results but also allows us to analyze the exciton states in more detail. We find four bound exciton states below the single-particle gap (gray line), with binding energies of 0.54 (1*g*), 0.50 (1*u*), 0.16 (2*g*) and 0.16 eV (2*u*) [24].

The first observation is the grouping of energies of the (1*g*, 1*u*) and (2*g*, 2*u*) states, respectively. This can easily be rationalized within a simplified cylindrical model, which describes an electron and hole moving under attractive Coulomb interaction on a the surface of a cylinder. In this model, the Coulomb potential is given by $V(z,\theta,R) = \mathrm{e}^2/\varepsilon\sqrt{z^2 + R^2\cos^2(\theta/2)}$ with the relative coordinate (z,θ) and tube diameter 2*R*. We have numerically solved the Schrödinger equation for such a cylindrical geometry and find a lowest energy state with a symmetric exciton relative wave function $\psi_1(z)$ which is localized along the axis and essentially fully delocalized along the circumference of the tube. The next higher bound exciton state has an antisymmetric relative wave function $\psi_2(z)$, which is more delocalized along the tube axis. With an effective dielectric constant $\varepsilon \approx 10.5$ we obtain for the (6,4) tube an energy splitting between these states of 325 meV, matching the experimental value. The shape of the numerically calculated wave functions is similar to that of the trial functions, $\psi_1(z;a) = \exp(-a\,|\,z\,|)$ and $\psi_2(z;b) \simeq z\exp(-b\,|\,z\,|)$, used for approximate variational solution of this cylinder model reported in Ref. [11].

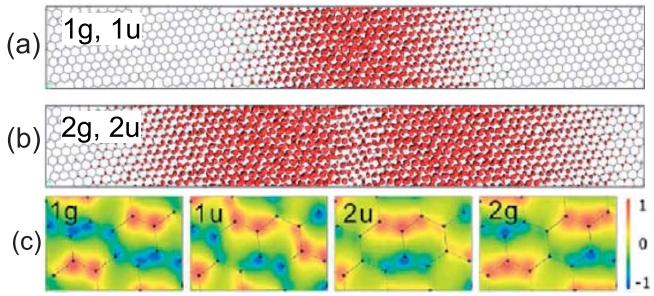

Fig. 7 (online colour at: www.pss-b.com) Lowest-energy excitonic wave functions for the (6,4) tube from *ab initio* calculations. The panels (a) and (b) correspond to the 1*g*, 1*u* and 2*g*, and 2*u* states, respectively, and show the probability of finding the electron on the tube surface when the hole is fixed at the center of the panel $z = 0$. The vertical direction corresponds to the circumference (2.1 nm) and the horizontal direction with a length of 15.9 nm to the tube axis. The bottom four panels (c) are blowups of the same states. They display the wave-function amplitude of the electron when the hole is placed in the center of the bond at $z = 0$ and show the parity under rotation by 180° about the *U* axis. The linear color scale is in arbitrary units.

In general, the overall shape of the exciton relative wave function predicted by this simplified cylinder model agrees quite well with the results of the full *ab initio* calculations. The lowest exciton wave function (1*g*, 1*u*) extends over several nm along the tube axis and is delocalized along the circumference [Fig. 7(a)]. The higher exciton states (2*g*, 2*u*) are more extended along the tube axis and have a nodal plane at $z = 0$, see Fig. 7(b). The calculated wave functions are thus Wannier-like and are only weakly dependent on the circumference direction.

In contrast to the simplified cylinder model, the *ab initio* calculations take the *local* electronic density for each carbon atom within the unit cell of the nanotube into account by using a large basis set of Gaussian orbitals for the individual atoms. A zoom into the wave functions of the different excitonic states is displayed in Fig. 7(c) and shows their symmetry with respect to π-rotation about the *U* axis (R_U). The four panels display the amplitude of the electron when the hole is placed in the center of the bond at $z = 0$. They show that the strongly bound low energy 1*g* and 1*u* states have different parities under R_U. This parity governs the optical dipole selection rules in carbon nanotubes: the *u* states are one-photon active, whereas *g* states are two-photon allowed. Also for the weakly bound excitons with a more delocalized relative wave function, we find a splitting into a pair of a (weakly) one-photon active 2*u* and a two-photon active 2*g* state.

These results suggest that the 1*u* exciton state dominates the optical absorption spectra of carbon nanotubes. The most strongly bound 1*g* exciton state, however, is optically inactive in one-photon absorption and weak in two-photon absorption [8]. Assuming a fast relaxation from the bright 1*u* into the dark 1*g* state, dark exciton states might explain the short luminescence lifetime [26] and small luminescence quantum yield in carbon nanotubes which is observed even at low temperatures. Additional time-resolved studies should be able to give insight into the microscopic physical mechanism underlying this exciton relaxation.

The calculations predict that the 1*g* state is only weakly two-photon active. Since its observation in two-photon photoluminescence spectra requires exciton relaxation into the higher lying optically 1*u* state, it is unlikely to be observable in such experiments. The application of sufficiently strong magnetic fields, however, induces a mixing of dark and bright states and a transfer of oscillator strength to the optically forbidden 1*g* state. Indeed recent magneto-optical experiments give experimental evidence for the presence of these optically dark states, the field-induced state mixing and the transfer of oscillator strength. Our theoretical model shows that the 2*g* exciton resonance dominates the experimental two-photon luminescence spectra. From the energy splitting between 2*g* and 1*u* states, the exciton binding energy can be derived provided that an appropriate model for the Coulomb interaction and the dimen-

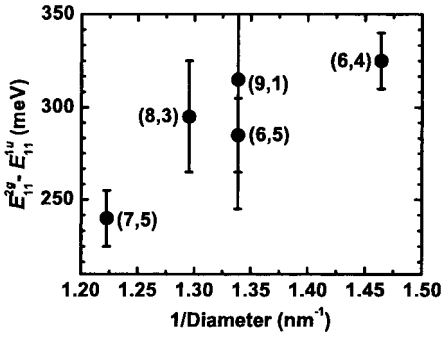

Fig. 8 Energy splitting between two-photon allowed 2*g* and the and one-photon allowed 1*u* exciton state as a function of the inverse diameter of the nanotube.

sionality of the excitonic wave function is used. The outlined cylinder gives good agreement with both experiment and first principle calculations and thus makes a prediction for the dependence of the exciton binding energy on the nanotube geometry.

Both the cylinder model and previous theoretical work [7–9] predict that the exciton binding energy is inversely proportional to the tube diameter. In addition, the energy should also depend on the family index [25] $\nu = (n_1 - n_2) \bmod 3 = \pm 1$, with larger binding energies E_{11}^b for $\nu = -1$ tubes than for $\nu = +1$ tubes with similar diameter [7, 8]. Our experimental results (Fig. 8) show indeed an overall decrease for larger tube diameters. The tubes in our experiment have $\nu = -1$, except for the (6,5) tube. It has the same diameter as the (9,1) tube, but a lower binding energy. Our data support the predicted trends. This is consistent with a very recent study of structural effects on exciton binding energies [28], which finds that the inverse proportional relation between exciton binding energy and tube diameter holds well for tubes with diameters between 0.8 and 1.2 nm.

In conclusion, we have studied excitonic effects on the linear and nonlinear optical spectra of carbon nanotubes both experimentally and theoretically. Our results clearly identify the optically relevant excitonic states and evidence exciton binding energies of 300 to 500 meV, much larger than the thermal energy at room temperature. This large exciton binding energy and the ability to control the nanotube diameter by studying nanotubes with well defined chiralities, makes carbon nanotubes important model systems for quasi-one-dimensional nanostructures, in particular as soon as disorder and defect effects on the optical spectra are better understood and the luminescence yield is enhanced. We anticipate that a detailed understanding of excitonic correlations in nanotubes will be important in tailoring the optical properties of single-walled carbon nanotubes.

Acknowledgements This work was supported in part by the DFG (SFB296), by an INFM Supercomputing grant at Cineca (Italy), by the RTN EU Contract "EXCITING" No. HPRN-CT-2002-00317, and by the Engineering and Physical Sciences Research Council (EPSRC). We thank A. Calzolari and G. Bussi for helpful discussions.

References

[1] M. J. O'Connell, S. M. Bachilo, C. B. Huffman, V. C. Moore, M. S. Strano, E. H. Haroz, K. L. Rialon, P. J. Boul, W. H. Noon, C. Kittrell, J. Ma, R. H. Hauge et al., Science **297**, 593 (2002).
[2] S. M. Bachilo, M. S. Strano, C. Kittrell, R. H. Hauge, R. E. Smalley, and R. B. Weisman, Science **298**, 2361 (2002).
[3] S. Reich, C. Thomsen, and J. Maultzsch, Carbon Nanotubes: Basic Concepts and Physical Properties (Wiley-VCH, Berlin, 2004).
[4] T. Ando, J. Phys. Soc. Jpn. **66**, 1066 (1997).
[5] E. Chang, G. Bussi, A. Ruini, and E. Molinari, Phys. Rev. Lett. **92**, 196401 (2004).
[6] C. D. Spataru, S. Ismail-Beigi, L. X. Benedict, and S. G. Louie, Phys. Rev. Lett. **92**, 077402 (2004).
[7] V. Perebeinos, J. Tersoff, and P. Avouris, Phys. Rev. Lett. **92**, 257402 (2004).
[8] H. Zhao and S. Mazumdar, Phys. Rev. Lett. **93**, 157402 (2004).
[9] C. L. Kane and E. J. Mele, Phys. Rev. Lett. **93**, 197402 (2004).

[10] F. Rossi and E. Molinari, Phys. Rev. Lett. **76**, 3642 (1996).
[11] J. Maultzsch, R. Pomraenke, S. Reich, E. Chang, D. Prezzi, A. Ruini, E. Molinari, M. S. Strano, C. Thomsen, and C. Lienau, Phys. Rev. B **72**, 241402(R) (2005).
[12] F. Wang, G. Dukovic, T. F. Heinz, and L. E. Brus, Science **308**, 838 (2005).
[13] Z. J. Wang, H. Pedrosa, T. Krauss, and L. Rothberg, Phys. Rev. Lett. **96**, 047403 (2006).
[14] R. Rinaldi, R. Cingolani, M. Lepore, M. Ferrara, I. M. Catalano, F. Rossi, L. Rota, E. Molinari, and P. Lugli, Phys. Rev. Lett. **73**, 2899 (1994).
[15] M. Damnjanović, I. Milošević, T. Vuković, and R. Sredanović, Phys. Rev. B **60**, 2728 (1999).
[16] H. Telg, J. Maultzsch, S. Reich, F. Hennrich, and C. Thomsen, Phys. Rev. Lett. **93**, 177401 (2004).
[17] J. Maultzsch, H. Telg, S. Reich, and C. Thomsen, Phys. Rev. B **72**, 205438 (2005).
[18] V. Perebeinos, J. Tersoff, and P. Avouris, Phys. Rev. Lett. **94**, 027402 (2005).
[19] X. Qiu, M. Freitag, V. Perebeinos, and P. Avouris, Nano Lett. **5**, 749 (2005).
[20] L. Hedin, Phys. Rev. **139**, A796 (1965).
[21] L. Benedict, E. Shirley, and R. Bohn, Phys. Rev. Lett. **80**, 4514 (1998).
[22] S. Albrecht, L. Reining, R. Del Sole, and G. Onida, Phys. Rev. Lett. **80**, 4510 (1998).
[23] A. Ruini, M. J. Caldas, G. Bussi, and E. Molinari, Phys. Rev. Lett. **76**, 206403 (2002).
[24] Binding energies are defined with respect to the onset of the single-particle continuum (gray line in Fig. 3).
[25] S. Reich and C. Thomsen, Phys. Rev. B **62**, 4273 (2000).
[26] A. Hagen, M. Steiner, M. B. Raschke, C. Lienau, T. Hertel, H. Qian, A. J. Meixner, and A. Hartschuh, Phys. Rev. Lett. **95**, 197401 (2005).
[27] S. Zaric, G. N. Ostojic, J. Shaver, J. Kono, O. Portugall, P. H. Frings, G. L. J. A. Rikken, M. Furis, S. A. Crooker, X. Wei, V. C. Moore, R. H. Hauge, and R. E. Smalley, Phys. Rev. Lett. **96**, 016406 (2006).
[28] G. Dukovic, F. Wang, D. Song, M. Y. Sfeir, T. F. Heinz, and L. E. Brus, Nano Lett. **5**, 2314 (2005).

